Spatio-Temporal Dynamics of Hypoxia during Radiotherapy

Harald Kempf[1,2], Marcus Bleicher[2], Michael Meyer-Hermann[1,3] *

1 Department of Systems Immunology and Braunschweig Integrated Centre of Systems Biology, Helmholtz Centre for Infection Research, Braunschweig, Germany, **2** Frankfurt Institute for Advanced Studies, Frankfurt, Germany, **3** Institute for Biochemistry, Biotechnology and Bioinformatics, Technische Universität Braunschweig, Braunschweig, Germany

* michael.meyer-hermann@theoretical-biology.de

Abstract

Tumour hypoxia plays a pivotal role in cancer therapy for most therapeutic approaches from radiotherapy to immunotherapy. The detailed and accurate knowledge of the oxygen distribution in a tumour is necessary in order to determine the right treatment strategy. Still, due to the limited spatial and temporal resolution of imaging methods as well as lacking fundamental understanding of internal oxygenation dynamics in tumours, the precise oxygen distribution map is rarely available for treatment planing. We employ an agent-based *in silico* tumour spheroid model in order to study the complex, localized and fast oxygen dynamics in tumour micro-regions which are induced by radiotherapy. A lattice-free, 3D, agent-based approach for cell representation is coupled with a high-resolution diffusion solver that includes a tissue density-dependent diffusion coefficient. This allows us to assess the space- and time-resolved reoxygenation response of a small subvolume of tumour tissue in response to radiotherapy. In response to irradiation the tumour nodule exhibits characteristic reoxygenation and re-depletion dynamics which we resolve with high spatio-temporal resolution. The reoxygenation follows specific timings, which should be respected in treatment in order to maximise the use of the oxygen enhancement effects. Oxygen dynamics within the tumour create windows of opportunity for the use of adjuvant chemotherapeutica and hypoxia-activated drugs. Overall, we show that by using modelling it is possible to follow the oxygenation dynamics beyond common resolution limits and predict beneficial strategies for therapy and *in vitro* verification. Models of cell cycle and oxygen dynamics in tumours should in the future be combined with imaging techniques, to allow for a systematic experimental study of possible improved schedules and to ultimately extend the reach of oxygenation monitoring available in clinical treatment.

Introduction

Hypoxia plays a pivotal role in the development and progression of cancer, as it is directly connected to central phenomena such as quiescence, changes in the cell metabolism, altered motility and treatment resistance [1, 2]. As a consequence, the oxygenation of tumours is a major

determinant for their aggressiveness, invasive potential and a predictive factor for the outcome of therapies [3–5]. While the persistent absence of oxygen in tumours can have negative effects on treatment, the natural and treatment-induced spatio-temporal dynamics of oxygenation also are of importance. Cyclic fluctuations of hypoxia have been shown to exert a strong influence on angiogenesis, radiosensitivity and gene expression of tumours [4, 6, 7].

This wide range of oxygen-related effects makes it desirable to include the oxygenation status of tumours in treatment planing. While hypoxia has a detrimental effect on radiotherapy and common chemotherapies, it can allow for the targeted use of hypoxia-specific therapies such as hypoxia-selective cytotoxins or bacterial lysis [8, 9]. Detailed information on the oxygen distribution within the tumour volume is thus necessary, in order to predict the effectiveness and schedule the exact combination of therapies.

An upcoming clinical tool for hypoxia detection is positron emission tomography (PET) which has a typical resolution of about 5mm in clinical settings [10]. As the hypoxic substructures in tumours are much smaller, this resolution limit implies that the micro-structure of hypoxia within a single voxel can not be effectively used to predict the therapy response and reoxygenation dynamics. Hypoxic areas in tumour tissue are often patterned on a scale of the inter-capillary distance of about 200–300 μm [11, 12]. Examples of this patterning have been observed with a range of different methods and in different tissues as for example in PC-3, EMT6 and 16C tumours [13], melanoma xenografts [14, 15] and in glioma (LN229) [16]. While the exact intercapillary distance can vary between tumour types and macroscopic regions, there is always an overall patterning as a results of the vascular structure. This self-similarity of macroscopic tumours makes it possible to study hypoxia by using tumour spheroids as a model for the tumour microregions in between capillaries. Spheroid cultures of cells posses a range of characteristics which correspond to *in vivo* tissues, most importantly the realistic mass transfer gradients of nutrients. Accordingly, they can be used as a model system to study basic reoxygenation dynamics in regards to the diffusion-based sources of hypoxia [17].

The imaging voxel size is of great importance as each voxel will contain a mixture of hypoxic and oxygenated cells, which will typically not be separated by resolutions in the order of 1mm. Tumour areas which appear to be non-hypoxic according to thresholding-methods can thus in reality contain significant hypoxic sub-regions which can drastically alter the treatment outcome [18]. As a consequence, the obtained PET data is partially unsuitable for the use in dose-painting calculations as it may lead to increased survival in hypoxic hot spots [18].

As neither patients nor tumours are static systems, insight into the oxygen dynamics in response to treatment is required on a microscopic and macroscopic scale, in order to identify local hypoxic areas and accordingly adapt the treatment schedules. Single measurements of the oxygen distribution or vascular structure are not sufficient for treatment planing due to the spatial and temporal dynamics of hypoxia [19]. Because of the current limits in temporal and spatial resolution, imaging of hypoxia can only assess the oxygenation on a coarse, thresholded level at few time-points during treatment, sometimes just characterising a whole tumour as "hypoxic" or "normoxic" [20]. This data basis is not satisfactory for efficient treatment design, because, as emphasised by this work, hypoxia is a phenomenon which has a pronounced structure on a scale below standard spatial and temporal imaging resolution.

Repeated hypoxia-imaging at selected time-points is required and must be combined with a model that can describe oxygen dynamics in the inter-imaging time periods and on spatial scales below the imaging resolution. Mathematical and computational modelling can provide the required insights and permit the investigation of the oxygenation dynamics under a wide range of assumptions. When combined with clinical imaging, the results of models can thus be used to include the oxygenation effects below the imaging resolution into treatment planing,

and thus to complete the data basis for adaptive therapies until better imaging techniques become available.

Sources, types and scales of hypoxia

The delivery of oxygen to tissue *in vivo* or *in vitro* has a multitude of facets. Three main mechanisms for the development of hypoxia can be coarsely distinguished: limited diffusion range, vessel occlusion and insufficient vascularisation [21].

The natural diffusion range of substances in a breathing tissue will lead to a critically low concentration of oxygen at a distance of more than approximately 100–200 from a capillary. If the distance is increased due to excessive growth of the tissue, which is not supported by the formation of new vessels, chronically hypoxic areas will form as illustrated in Fig 1. Within tumours the vascular density is known to be decreased with typical inter-capillary distances of about 300 μm [11, 12]. As these distances exceed the diffusion range, this leads to chronic hypoxia and a patterning of hypoxic regions with about 200 diameter [1, 13]. Suboptimal architecture of the vessels in angiogenesis can furthermore decrease the diffusion range and lead to a lacking supply in macroscopic regions of tissue [22].

Large parts of hypoxia dynamics are related to blood flow in the vascular network. As flow resistance in vessels is inversely proportional to the fourth power of the vessel diameter, small changes by vasomotion can cause large fluctuations in the network [4, 23]. Accordingly, vessel occlusions due to pressure, blood clotting, inflammation, and damage can furthermore influence blood flow and induce transient hypoxia also on a large spatial scale.

While the smallest spatial scale of hypoxia is on the order of 100 μm, temporal variations of pO_2 in mouse models have been observed with periodicities of minutes, even in the absence of treatment [6]. Changes in perfusion, erythrocyte flux and vascular occlusion can occur within minutes and hours, while changes in the vascular network and angiogenesis usually take place on a scale of days. Fluctuations can be as extreme as maximal 18-fold changes in pO_2 which
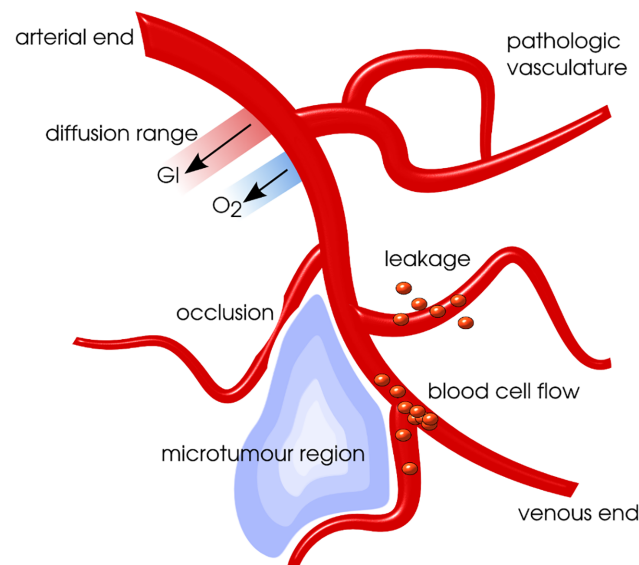

Fig 1. Hypoxia sources in tumours and diffusion range of substances. Illustration of selected hypoxia sources and a hypoxic tumour micro-region in tumour tissue. Hypoxic micro-regions will usually form a characteristic tiled pattern throughout a tumour. For *in vitro* examples of patterning in tumour xenografts see Fig 2 in reference [13].

have been observed with cyclic patterns on the scale of only minutes even in undisturbed tumours [7, 24].

Changes in vessel flow are hard to track and describe which makes acute, perfusion-driven hypoxia unpredictable [25]. The diffusion-based hypoxia on the other hand can be investigated in spheroid systems and modelled in a straightforward approach.

Effects of hypoxia on therapy and treatment planning

Oxygen is of special importance for the effectiveness of radiotherapy, as radiation damage to cells is drastically reduced under hypoxic conditions [25]. This oxygen enhancement effect (OER) is present in every tumour region of low oxygen concentration and will only vanish above an oxygen partial pressure of about 10 mmHg pO_2, a concentration which is typically used as definition of the hypoxia threshold [26]. The according oxygen modification of radio-sensitivity for the clinical standard, the linear-quadratic model (LQ), was first proposed in 1956 [27] and is now commonly used in treatment planing [25, 28]. While oxygen enhancement is especially important for radiation with low linear energy transfer (LET) such as x-rays (with a typical LET of $2 keV/\mu m$), it is also relevant in modern therapies which employ high-LET radiation in extended Bragg peaks [29].

In order to cancel out the effects of oxygen-shortage, the dose to hypoxic tumour regions is often increased in radiotherapy plans or modified in dose-painting approaches. This approach however depends critically on the spatio-temporal resolution of information on the oxygen kinetics. As the location of hypoxic areas is likely to change on a day-to-day basis, prescription plans might already be invalidated as soon as they are started, if the resolution is not sufficient [30].

As the action of a wide range of drugs will also depend on the availability of oxygen, the importance of oxygen dynamics in treatment planing extends also to radio-chemo schedules and pure chemotherapy [3]. Furthermore, in drug delivery the treatment-induced changes in diffusivity of the tumour tissue will be of great importance [31].

Detection and measurement of hypoxia

As the success of therapies to a large degree depends on an accurate imaging of hypoxia, the detection and quantification of hypoxia is continuously becoming more precise and cost-efficient [32, 33]. For *in vitro* experiments a range of methods such as polarographic needle measurements or immunostaining allow for dynamic, quantitative or large-scale assessment of hypoxia in tissue. While some of these techniques are also suitable for *in vivo* use, the availability of techniques is more limited, especially if non-invasive methods are preferred [34, 35].

Positron emission tomography (PET), as a clinical tool for hypoxia detection, suffers from both relatively low spatial and temporal resolution. Low tumour to blood ratios of tracers and long scan times limit the temporal resolution to 3 hours [30]. This implies that the time-point of PET observation is critical for the assessment of the true oxygenation, especially in tumours under the effects of treatment [10]. Relatively long PET scan times lead to motion averaging of heterogeneity and fast tumour hypoxia. Also spatially the resolution of PET imaging is quite limited. A clinical resolution of about 5 mm^3 voxel size is typical, while advanced systems will be able to achieve resolutions of 1 mm^3 [10].

In summary, PET measurements can usually only provide integral, time-averaged values of local oxygen concentration and will suffer from blurring effects and background noise during imaging. As a consequence, they cannot capture the micro-structure of hypoxia, which is below the typical clinical resolution, but which is of vital important for the response to therapy and the subsequent reoxygenation dynamics.

Newer imaging techniques, as for example electron paramagnetic resonance imaging (EPRI), can provide absolute oxygen concentrations from three-dimensional systems with a resolution of 1 mm and 2 min [6]. However, EPR imaging is currently not employed in clinical settings and will require further development to become widely available. In an experimental setting, EPR imaging allows for extreme temporal and spatial resolution which can be used to assess the predictions of oxygen dynamics models and to increase their accuracy by tuning of model parameters. Furthermore, a range of innovative high quality imaging and measuring techniques are under development [36, 37], which facilitate data gathering in spheroids and make it possible to image in *in vivo* systems [38, 39].

For clinical practice, a non-invasive, high-frequency, quantitative imaging technique is desirable, in order to track hypoxic dynamics over minutes and days [6]. Lin and Hahn call for a repeated combined PET/CT imaging during therapy in order to verify the tumour response in hypoxia and to use the information for an accurate dose painting and escalation in acutely hypoxic regions [30].

A connection between imaging and modelling has to be established in order to predict oxygen dynamics beyond available imaging resolution. An example of an observable which can connect model predictions of hypoxia dynamics and experimental observations is the uptake of tracers in PET-imaging [30].

Predicting oxygen dynamics *in silico*

The chronic hypoxia in a tumour spheroid is spatially similar to hypoxia in an inter-capillary microregion of tumour tissue, as is illustrated in Fig 1. Accordingly, within the current work, the modelling of hypoxia is not performed on the level of averaged voxels and with timesteps of hours, but instead for a small nodule with a diameter of 1000 μm. Thus the system provides an intrinsic dynamic of tumour hypoxia, which is in the same form repeated as a pattern within the inter-vascular spaces of *in vivo* tumours.

This approach is drastically different from alternative *in silico* models of tumour hypoxia which typically employ averaged 1D cell populations [40, 41], 2D lattice-based cellular automata [42, 43], restrain themselves to analytical solutions of oxygen availability [44] or known micro-vessel distribution [45]. A range of models has addressed the issue of tissue oxygenation measurement with polarographic needles in regards to reliable and accurate measurements [46, 47], while relying on a known, pre-imposed or measured vascular network. Also the effects of the vascular network itself have been studied in regards to growth-inhibiting and -promoting effects [48].

Most existing models for tumour hypoxia make use of large, averaged voxels in order to represent a subset of individual cells, are restricted to a regular grid with rather low cell numbers (often in the order of only 10000 cells), impose strong symmetry assumptions to derive analytical solutions or use extremely large timesteps on the order of hours or days [49]. In contrast to this approaches our model will employ a lattice-free 3D environment, in which a high number of individual cells (up to 1000000) is represented on a timescale of seconds and can interact with a high-resolution diffusion solver of 71^3 grid nodes, which also takes into account the local variability of the diffusion coefficient in dependence on the cell density. A range of alternative high-performance on- and off-lattice models could be suitable targets to be employed in a similar type of hypoxia modelling by introduction of nutrient diffusion into the according models [50, 51].

We will address the previously unregarded timescale of tumour hypoxia and oxygenation in the range of minutes and hours and show that treatment-induced changes will affect the outcome in fractionated radio- or chemotherapy treatment protocols. Our focus will rest on the local, high-resolution dynamics of oxygenation both in space and time. In contrast to the usual

perception, we will demonstrate that the "chronic" diffusion-limited hypoxia can lead to fast and drastic changes in tumour oxygenation, which are—to a large degree -predictable in contrast to other sources of hypoxia.

Methods

Cell-based spheroid growth model

A three-dimensional, single-cell based model is used in order to track the growth of tumour spheroids from a small number of seeder cells and to monitor their oxygenation response in reaction to therapeutic approaches [52, 53]. The spatial arrangement of cells as tissue is represented in a Voronoi-Delaunay model [54–56] and the adhesive-repulsive interaction between cells is modelled using the Johnson-Kendal-Roberts approach [57, 58]. The simulation relies on experimentally measured cell parameters from EMT6 and V79 cells in order to achieve a realistic implementation of a generic cancer cell.

Cells in the simulation are subject to a cell cycle regulation, as shown in Fig 2(a), and will accordingly react to the realistic nutrient and pressure gradients that develop in the growing
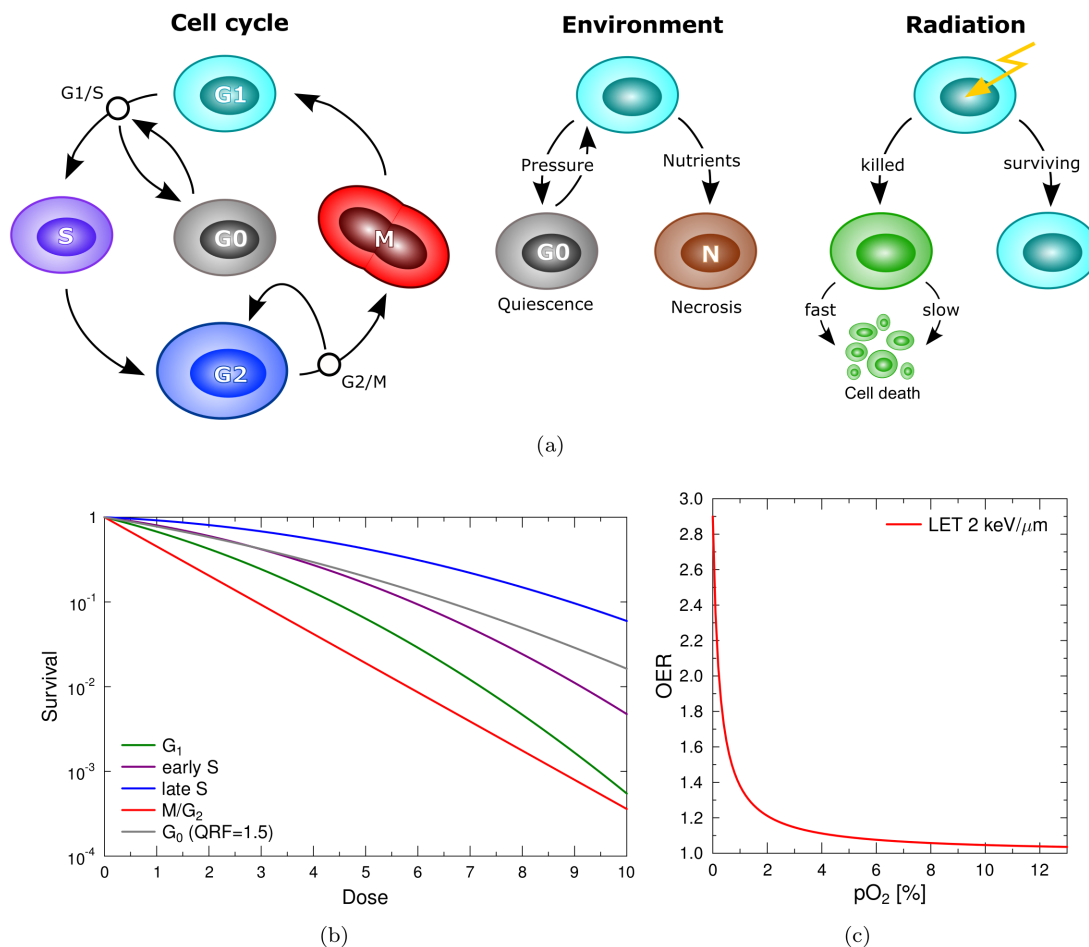

Fig 2. Regulation of the cell cycle and radiation reaction. (**a**) Overview of the cell cycle regulation, cell responses to environmental factors and radiation. (**b**) Survival curves for cells in specific cycle phases and with increased radioresistance due to quiescence, as described with the linear-quadratic model Eq 5. (**c**) Dependency of the oxygen enhancement ratio on the local oxygen concentration employed in order to alter the radiation response for hypoxic cells according to Eq 6, calculated according to equation 8 from [59].

doi:10.1371/journal.pone.0133357.g002

Table 1. Listing of parameters used in the model. Further parameters and sources for cell interaction, nutrient diffusion and consumption can be found in [52] and [56].

Parameter	Value	Sources and remarks
Diffusion nodes	71	per dimension
System size	1000 µm	cubic lattice
Glucose boundary conc.	5 mM	capillary blood
Oxygen boundary conc.	0.13 mM	[64]
Update intervall	10 min	
Glucose diffusion coefficient water $D_{H_2O}^{G1}$	690 µm^2/s	[65]
Glucose diffusion coefficient tissue D_{Tis}^{G1}	105 µm^2/s	[66]
Oxygen diffusion coefficient water $D_{H_2O}^{O_2}$	3300 µm^2/s	[67]
Oxygen diffusion coefficient tissue $D_{Tis}^{O_2}$	1750 µm^2/s	[67]
Initial cell radius (start G1)	7.94 µm	[63]
Final cell radius (end G2)	10 µm	[63]
avg. necrosis and apoptosis duration τ_n, τ_A	24 h, 12 h	[68–70]
Starvation glucose level	0 mM	growth fit
Quiescence critical pressure P_{crit}	200 Pa	[71], growth fit
Hypoxia threshold	0.014 mM	[26]
Active glucose consumption	180 amol cell^{-1} s^{-1}	[60, 63]
Quiescent glucose consumption	130 amol cell^{-1} s^{-1}	[60, 63]
Active oxygen consumption	83 amol cell^{-1} s^{-1}	[63]
Quiescent oxygen consumption	49 amol cell^{-1} s^{-1}	[63]
acute death chance AC	0.66	[52] [53]
mitotic mismatch rate MM	0.3	[52] [53]
LQ-model α_{G1}, β_{G1}	0.351, 0.04	[25, 72]
LQ-model α_S, β_S	0.1235, 0.0285	[25, 72]
LQ-model $\alpha_{M/G2}$, $\beta_{M/G2}$	0.793, 0	[25, 72]
Quiescence resistance factor QRF	1.5	[73, 74]
Maximum oxygen enhancement O_{max}	2.9	[29]
OER half-life concentration	0.0052 mM	[25]

doi:10.1371/journal.pone.0133357.t001

tumour spheroid. Quiescence of cells is by default triggered if a cell is subject to a critically high pressure P_{crit} of more than 200 Pa from neighbouring cells at the G1/S-checkpoint. The cell is released back into the active cycle once the pressure decreases to sub-critical levels. Cells are considered to be fully tolerant to anoxia during the total time of modelling. In contrast to this, a local depletion of glucose leads to the starvation of cells and accordingly triggers necrosis.

Cell nutrient consumption

Cells consume oxygen and glucose from a diffusion system which is superimposed on the spatial tumour model. As the nutrient uptake is more regulated by metabolic needs than by environmental factors, nutrients are taken up by a cell independently from the concentration. This implies zero-order uptake kinetics, in which cells consume a constant amount of nutrients per time interval, according to experimentally measured consumption rates (as indicated in Table 1 [52, 60]).

For cells in the quiescent state the oxygen consumption has been demonstrated to be decreased [61, 62]. To capture the reduced metabolic needs of quiescent cells, their consumption rates for oxygen and glucose in the model were decreased accordingly as measured in [63] and indicated in Table 1.

Diffusion modelling

Nutrients enter the spheroid by diffusion through its boundary surface and are locally consumed by cells, which can be described by the diffusion equation with sink term $Q(x, t)$

$$\frac{\partial C(x, t)}{\partial t} = \frac{\partial^2}{\partial x^2}\left(D(x, t)C(x, t)\right) + Q(x, t).$$ (1)

The boundary surface is kept at a constant nutrient concentration, as a sufficiently well-mixed reservoir of nutrients is assumed to be available for support from the blood stream. As the tumour changes in size and shape, the boundary surface is adapted so that any node outside the tumour which is not occupied by cells will become part of the boundary. While a common simplification in diffusion modelling is the assumption of a constant diffusion coefficient [47, 75], it is necessary to consider a local variation of the diffusion coefficient. As the diffusion coefficient for substances in water differs greatly from the diffusion in tissue, this step is vital in order to obtain a reliable result. This is especially true when the integrity and density of the tissue under observation will be altered by therapeutic approaches, due to dissolution of dead cells. As a consequence, the diffusion coefficient within the system is space-dependent and will vary between the measured coefficients for diffusion in water D_{H_2O} and tissue D_{Tis}

$$D(x, t) = D_{Tis} + (D_{H_2O} - D_{Tis})\frac{\varrho(x, t)}{d_{max}}$$ (2)

depending on the local cell density $\varrho(x, t)$ (calculated as cells per volume) and the maximum density in a dense packing d_{max} (determined from a compressed cell mass in the system). This approach is a novelty and improvement of the diffusion system in comparison to other diffusion models. A linear dependency of the diffusion coefficients on local density is assumed as first approximation. With this addition the diffusion equation of the system becomes

$$\frac{\partial C(x, t)}{\partial t} = \frac{\partial}{\partial x}\left(D(x, t)\frac{\partial C(x, t)}{\partial x}\right) + Q(x, t)$$ (3)

where for the steady state case the assumption $\frac{\partial C(x,t)}{\partial t} \approx 0$ is valid. This leaves a Poisson-type problem for the system

$$\frac{\partial}{\partial x}\left(D(x)\frac{\partial C(x)}{\partial x}\right) = -Q(x).$$ (4)

This reaction diffusion equation is numerically solved in a finite difference form, using the Crank Nicholson scheme under careful implementation of mechanisms, which guarantee the validity and stability of the solution, such as an adaptive maximum stepsize and sanity checks. By default, a pseudo-steady-state approximation is employed in order to recalculate the steady-state of diffusion in fixed time steps using an unconditionally stable biconjugate gradient method. This approximation is possible as the non-stationary evolution time of the system is very short [45, 76].

The diffusion of glucose and oxygen is modelled on a cubic reaction diffusion solver system of 1 mm edge length using 71 nodes per dimension. Any off-grid concentration is retrieved or stored in the solver using trilinear interpolation. Nutrient conditions in regions of the system which are not occupied by cells are fixed to typical concentrations in arterial blood of 5 mM glucose and 0.13 mM oxygen [64]. For diffusion of substances in water and tumour tissue at 37°C the following coefficients are used: $D_{H_2O}^{G1} = 690 \ \mu m^2/s$ [65], $D_{Tis}^{G1} = 105 \ \mu m^2/s$ [66]

(EMT6 spheroid), $D_{\mathrm{H_2O}}^{\mathrm{O_2}} = 3300$ μm²/s [67], and $D_{\mathrm{Tis}}^{\mathrm{O_2}} = 1750$ μm²/s [67] (DS-Carcinosarcoma *in vivo*).

Reactions to irradiation

The total amount of cell death in response to a radiation dose is matched to experimental observations via the linear quadratic model for single cell survival [25, 28]. Cells use a representative *cell cycle phase-dependent* survival probability S_p to assess their survival in dependence of the radiation dose D:

$$S_p = e^{-(\alpha_p D + \beta_p D^2)} \tag{5}$$

As physiological example, α_p and β_p values of V79 hamster cells subjected to x-ray irradiation by Sinclair [72] are employed, as shown in Fig 2(b) (see also Table 1). These values reflect the typical behaviour of cells exemplarily, with high radioresistance in S-phase and high radiosensitivity in G2/M-phase. Since the radiation sensitivity of quiescent cells has been demonstrated to be lower than that of actively cycling cells, the effective dose to cells which are in quiescence is scaled down in the model using the quiescence resistance factor QRF = 1.5 [73, 74].

Cells committed to radiation-induced death are either killed immediately via an acute, fast death process (fatal damage with probability *AC*) or later in their cycle progression by delayed death (e.g. in response to mitotic catastrophe), as indicated in Fig 2. While marked as damaged, a cell is arrested once it reaches the G2/M checkpoint until it progresses to cell death with a "mitotic mismatch"-rate *MM*.

The radiosensitivity of cells decreases for critically low oxygen concentrations below 20–30 mmHg [25, 77]. These effects of local oxygenation on radiation damage are taken into account via the oxygen enhancement ratio (OER), which is formally defined as the ratio of doses needed to achieve a certain survival level in cells, either in normoxic conditions D_{ox} or under hypoxic conditions D_{hy}:

$$\mathrm{OER}(pO_2) = \frac{D_{\mathrm{hy}}}{D_{\mathrm{ox}}}\Big|_{\mathrm{same\ effect}} = \frac{O_{\max} \cdot pO_2 + H}{pO_2 + H} \tag{6}$$

Eq 6 implies a dependency which is determined by the maximum OER effect $O_{\max}$ and the pO_2 at half effect H in the commonly used parametrisation provided by Alper and Howard-Flanders [27]. The according maximum OER in V79 spheroid cells was measured to be 2.9 for X-rays (250kV) with an LET of 1.7keV/μm [29]. The employed oxygen enhancement for the simulation is shown in Fig 2(c) and calculated according to equation 8 from [59]. The half-life of oxygen enhancement is around 0.5% pO_2 [25]. The OER varies only mildly throughout the cell cycle between 2.3 for G2-cells and 2.8 for S-cells and consequently has been assumed to be cycle-independent.

Measuring of hypoxia and reoxygenation

The oxygenation status of all cells in the simulation is available as observable at all times. One of the measurables under investigation is the fraction of cells which are subjected to a local oxygen concentration below a defined threshold. Spatial profiles of oxygen concentration and the temporal evolution of the concentration at the centre of the tumour spheroid are also of interest, as they contain information on the localisation of hypoxic cells.

One of the non-invasive techniques employed in clinical settings is the monitoring of the oxygen concentration in the tumour via PET, which will typically yield spatially resolved images of the tumour volume with a voxel size of about 5mm^3. Below this level only time and

space-averaged data is usually obtained [10]. Consequently an integral measure of oxygen

$$P(t) = \int_{\text{Tumour}} C(x, t)\, d^3x \tag{7}$$

can be used to compare model predictions with experimental and clinical results.

The observable $P(t)$ is directly related to the oxygen-dependent tracer-quantity which is measured in PET-monitoring of tumour-subregions.

Results

Spheroid growth and rise of hypoxia

In silico spheroids were grown from 10 seeder cells, which were initially distributed randomly in the gap and synthesis phases of the cell cycle. Spheroids grew to a typical diameter of 700 μm after 14 days of proliferation. Steep oxygen and glucose gradients developed inside the spheroids as visualised in Fig 3. After about 9.5 days of growth, a hypoxic population developed as a result of the limited diffusion range of oxygen, followed by central anoxia after 10 days. Total glucose deprivation in the centre of the spheroid was observed after about 11 days and led to the onset of central necrosis (see Fig 3(c) and 3(d)). 12 days after seeding the relative distribution of cells in the cell cycle phases, as well as the oxygenation was sufficiently stable in order to study the reaction of the spheroid system to irradiation.

The observed diffusion range of substances in the spheroid corresponded well to experimental measurements and theoretical predictions (100–200 μm range *in vivo* [78, 79], 200 μm

(a) (b) (c) (d)
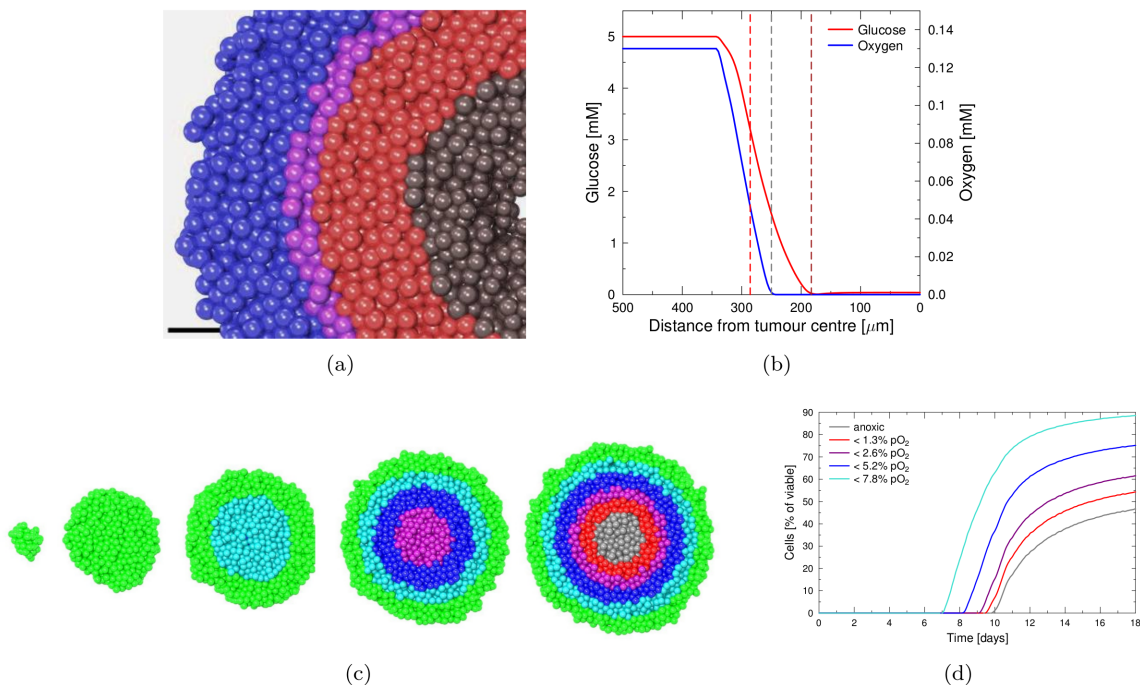
Fig 3. Distribution of nutrients in the spheroid and de-oxygenation during growth. (a) Central cut-section through an *in silico* EMT6 tumour spheroid after 12 days of growth. Normoxic cells (pO₂ > 2.5%) in blue, cells below 2.5% pO₂ in purple, below 0.5% in red and necrotic cells in grey. Slice thickness is 40 μm. Compare to the *in vitro* immunodetection of pimonidazole in hypoxic cells in the peri-necrotic regions of a tumour spheroids (T47D after 10–14 days of growth) in Fig 3a in [80] (bar size in both images 50 μm). **(b)** Lateral concentration profiles of glucose and oxygen. The higher reach of survival-promoting glucose will lead to the formation of an anoxic region (between grey and brown dashed line). Hypoxic cells will be found in low-oxygen regions (between red and grey dashed line) and normoxic cells beyond the red dashed line. Compare also reference [1]. **(c)** Central cut-section of 40 μm thickness through an *in silico* EMT6 tumour with oxygen-dependent staining after 2, 6.5, 8.3, 9.5 and 10.2 days of growth. Cell staining corresponds to the line color in graph (d) (green cells are above 7.8%pO₂). **(d)** Development of cell populations below defined oxygen concentrations in the spheroid as visualised in (c).

doi:10.1371/journal.pone.0133357.g003

range of O_2 predicted [75]). Fig 3(b) shows the diffusion range of oxygen and glucose in the spheroid at the 14th day of growth. While the central region was void of both oxygen and glucose, a large layer of viable but anoxic cells developed due to the larger range of survival-promoting glucose. A steep concentration gradient led from a hypoxic cell population up to the normoxic population at typical capillary blood concentrations on the surface of the spheroid.

A qualitative comparison of hypoxia *in silico* and *in vitro*, as in Fig 3(a) and Fig. 3a in [80], illustrates the histological correspondence of the tumour spheroid model to experimental spheroid systems.

Response to treatment and reoxygenation dynamics

Irradiation with 4Gy of x-rays drastically affected the oxygenation of the tumour and triggered a complex cascade of reactions, as illustrated in Fig 4. Cell death in response to the radiation dose led to a significant drop in the nutrient consumption density, which allowed for a far greater penetration depth of nutrients. In addition, the dissolution of dead cells decreased the tissue density and consequently led to a higher diffusion coefficient, which further increased the range of oxygen and glucose, as shown in Fig 5.

The observed increase in penetration depth of diffusing substances is illustrated in Fig 4(a). While directly prior to irradiation a large anoxic and hypoxic population was present in the inner region of the spheroid, anoxia was completely lifted already one hour after irradiation. The width of the cell layers which were subjected to high concentrations of oxygen accordingly increased throughout the tumour volume.

The dissolution of dead cells also led to a drop in the pressure on quiescent cells, which allowed for the re-entry of previously non-cycling cells into the active cycle. Through the associated increase in nutrient consumption, a fast re-depletion of nutrients was triggered.

As a result, the typical hypoxic fraction of cells drastically changed in response to irradiation. A slight increase in the fraction of hypoxic cells immediately after irradiation was observed, which was due to radioresistance of hypoxic cells that translated directly into a survival advantage (see dot marker in Fig 4(c)). As expected, this temporary increase was relatively higher for populations with lower oxygen concentration. In general, a full re-oxygenation of the tumour was observed. However, the concentration in inner regions of the spheroid was not lifted above the hypoxic threshold by a radiation dose of 4Gy, as is shown in Fig 4(e). Within 4 hours an anoxic population of 5% had reformed and after 15 hours levels of oxygenation were reached which were comparable to the pre-treatment situation. Due to the strong regrowth of the spheroid, an overshooting of consumption was observed, which decreased the availability of oxygen even below pre-treatment levels 19 hours post-radiation (see star in Fig 4(c)).

If the maximum oxygen enhancement ratio was set to unity ($O_{max} = 1$), thus mimicking the use of hypoxic sensitizers and effectively making radiation damage oxygen-independent, the reoxygenation response was drastically enhanced (compare Fig 4(a) and 4(b)). As hypoxic cells in the central regions of the spheroid were no longer subject to a survival advantage from their increased radioresistance, a higher fraction of cells was killed by irradiation.

The following increase in diffusivity and decrease in consumption led to a significantly higher influx of oxygen and a longer persistence of reoxygenation in the tumour. Consequently, irradiation with 4Gy fully re-oxygenated the tumour to a level which was well above the hypoxia threshold of 0.014 mM throughout the whole spheroid, as is shown in Fig 4(f). The reoxygenation persisted for 42h before pre-treatment levels of anoxia were reached again. Regrowth would at the same time increase the consumption density and decrease the diffusion coefficient, so that the re-depletion of oxygen was a very fast process.
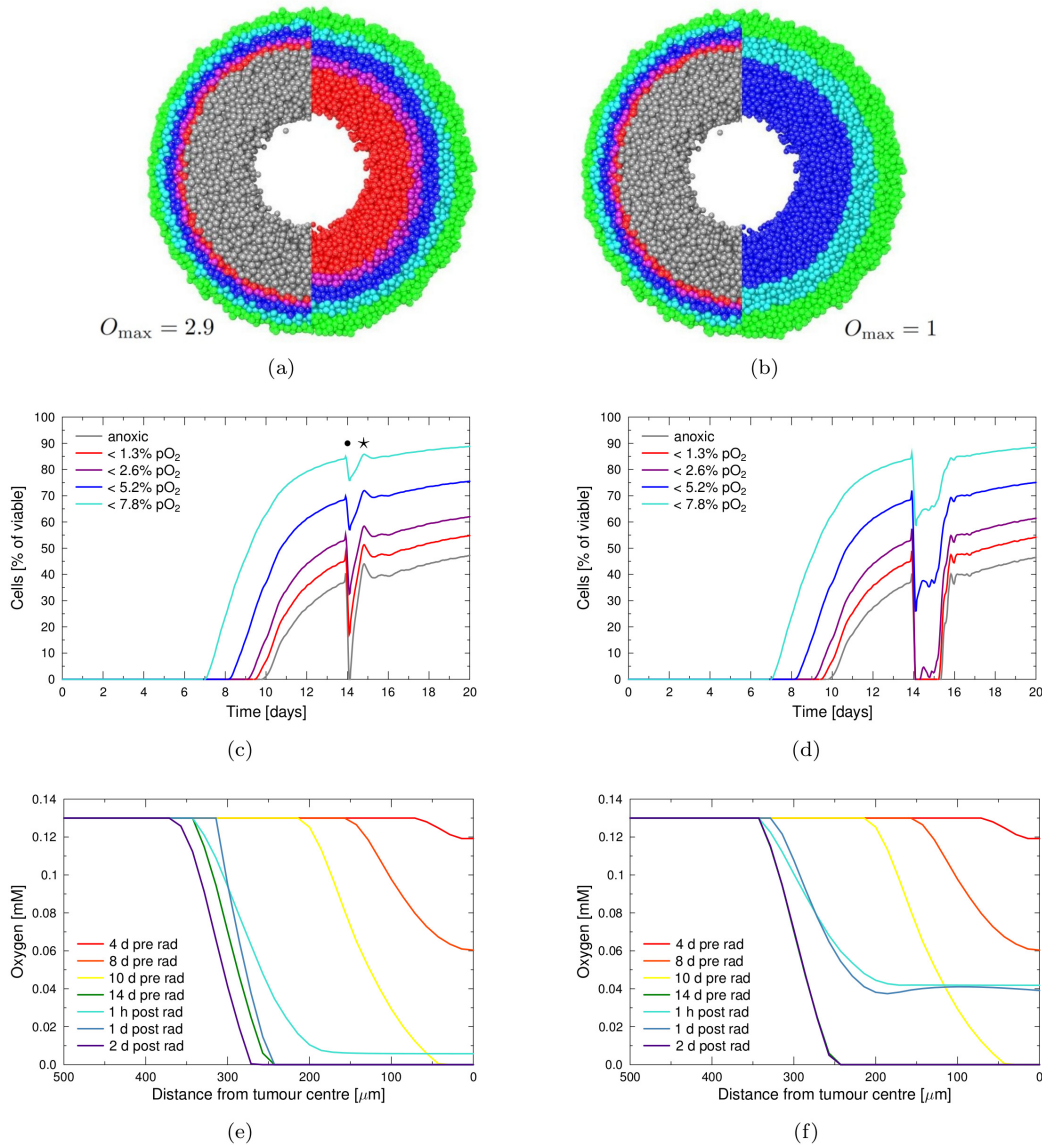
Fig 4. Reoxygenation of the spheroid in response to a single radiation dose. Irradiation has been performed with a dose of 4 Gy at day 14, either with normal oxygen enhancement ($O_{max} = 2.9$, left column) or with suppressed oxygen enhancement ($O_{max} = 1$, right column). **(a-b)** Pre- (left) and post-radiation (right) cutsection with oxygenation staining of cells as in Fig 3(c) and 3(d). **(c-d)** Fraction of cells which are subjected to different oxygen levels during growth and irradiation. Dot marker shows treatment-induced increase in hypoxic cells and star marker the regrowth-induced increase (refer to main text for details). **(e-f)** Lateral concentration profile of oxygen in the tumour spheroid at different time points during growth and treatment.

doi:10.1371/journal.pone.0133357.g004

Especially in the case of $O_{max} = 1$, local fluctuations in oxygenation could be observed, which were driven by the interplay of the re-entry of quiescent cells into the active cycle, the associated tumour regrowth, local nutrient depletion and necrosis. This dynamics led to a complex development of local oxygenation, as is visible in Fig 4(d) and visualised in S1 Fig.

PET comparison and optimal imaging

If local invasive techniques are available for assessment of the oxygenation during treatment, then the oxygenation profile can be compared quantitatively as in Fig 4(e). For non-invasive techniques on the other hand, only integral oxygen concentrations can be used for comparison.
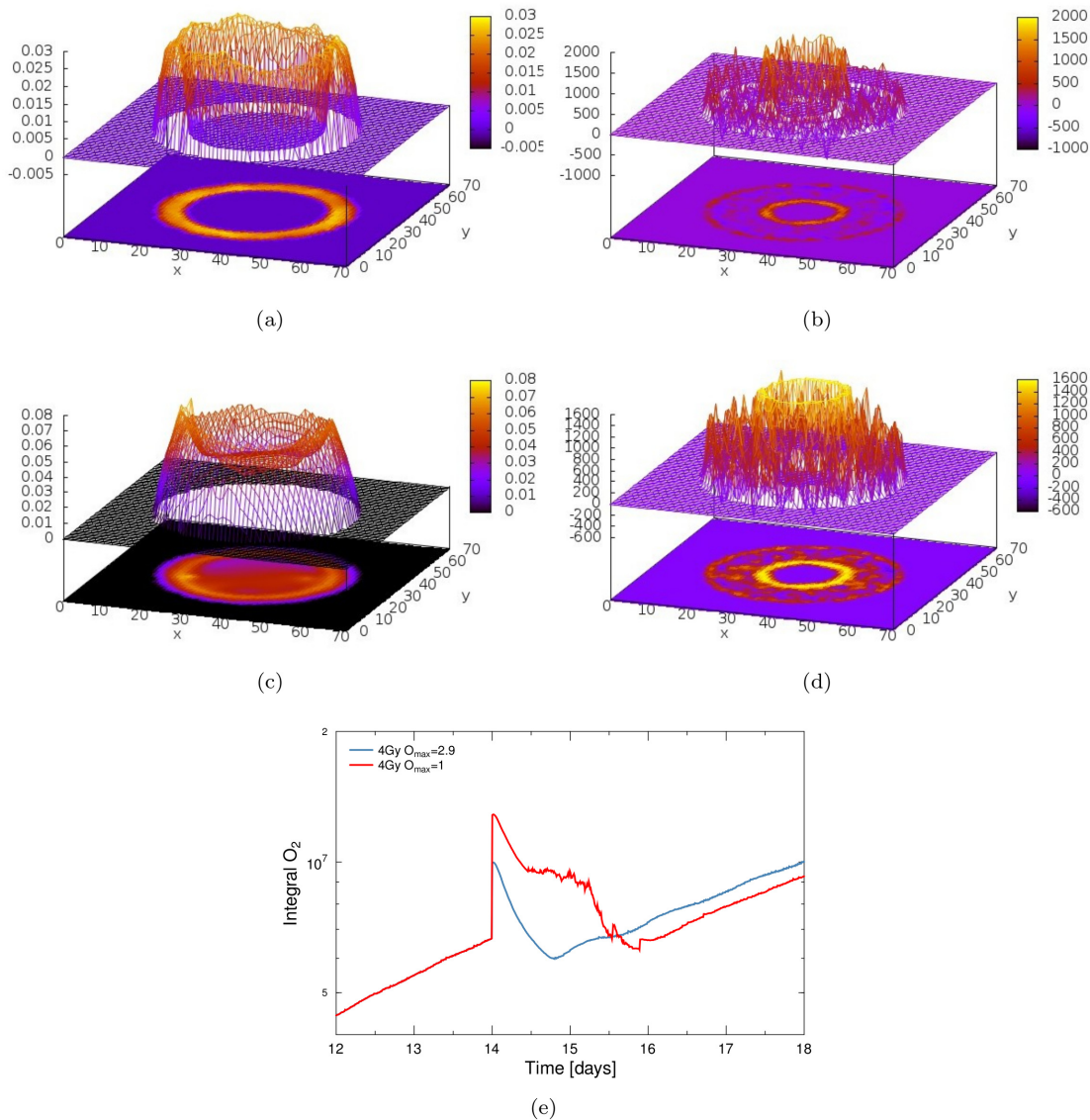
Fig 5. Changes in oxygenation and diffusivity in response to irradiation and integral oxygen concentration as PET-equivalent. (a-d) Change in the oxygen concentration (left column, difference in mM) and the density-dependent oxygen diffusion coefficient (right column, difference in μm^2/s) between a pre- and post-radiated tumour state. Visualisation shows the difference in a central cutslice of the diffusion system (x and y denote grid nodes over 1000 μm, z and the color palette illustrate the difference in the according units). **(a-b)** show the rise in local oxygen concentration and the increase in the diffusivity as difference between a pre-radiated state and 12 hours after irradiation with 4 Gy and O_{max} = 2.9, **(c-d)** for 4 Gy and O_{max} = 1 with 24 hours difference. The dissolution and permeabilisation of dead cells will lead to a significant rise of oxygen diffusion into the tumour bulk. This influx is in parts due to a lower local consumption but also due to local increase in tissue diffusivity. **(e)** Integral oxygen $P(t)$ in the tumour spheroid in response to a single irradiation dose of 4 Gy x-rays at day 14 with full or suppressed oxygen enhancement in effect. The integral signal can be quantitatively compared to PET signals.

Fig 5(e) shows a sample of the integral oxygen dynamics within the tumour spheroid. Radiation triggered a fast re-oxygenation in the tumour, which was expressed as a sudden rise in the integral amount of oxygen. If the typical oxygen enhancement effects were present, a smooth re-depletion of oxygen was observed over 16 hours. With suppressed oxygen enhancement the re-depletion signal was more complex and extended over almost 48 hours, due to severe damage to cells also in hypoxic areas.

Due to the micro-structure of the tumour tissue, the macroscopic, diffusion-related change in the PET-signal will contain a component which is a direct result of the change within each micro sub-volume (which in turn corresponds to the modelled tumour spheroid *in vitro*). Thus a part of the observed change in the PET-signal can be predicted and compared directly to experimental measurements.

While the local oxygen concentration naturally showed extreme fluctuations in response to irradiation, the integral oxygen measure also exhibited dynamics on a short timescale, as is visualised in Fig 5(e). This illustrates the critical importance of imaging timing, as assessment of oxygenation at transient extreme points can lead to false dose escalation and treatment planning.

Persistence of reoxygenation during repeated treatment and its impact on sequential therapies

Reoxygenation during the course of fractionated therapies is of great interest for treatment planing. Ideally, therapies achieve a lasting reoxygenation within a short time, as this enables following fractions to exploit the enhancing effects of oxygen. To allow for this effect, the reoxygenation must be persistent for a time period which is equal to, or greater, than typical clinical scheduling intervals.

Within the simulations the oxygenation response was identical upon repeated irradiation, provided that the interval between fractions was chosen larger than the typical time needed for re-establishment of a pre-treatment population of hypoxic cells. If treatment intervals were chosen smaller, consecutive fractions of radiation each affected a tumour which was not fully in equilibrium, but slightly more oxygenated than at the start of treatment. In consequence, a build-up of a lasting oxygenation could be achieved.

Typical scenarios for repeated radiation delivery are fractions of 2Gy every 24h in a conventional radiation schedule or 4Gy every 48h in a hypo-fractionated schedule. The according oxygenation dynamics within the simulation are shown in Fig 6 for clinical accelerated schedules without fractionation-pauses during the weekend. Repeated doses of 4Gy effectively cleared the tumour of hypoxic cells for extended time periods, prior to the administration of follow-up doses. After 48h a fast rise in the hypoxic fraction led to the loss of any oxygenation-advantage for treatment, as indicated in Fig 6(b). For lower doses, 2Gy per 24h, a short-lived reoxygenation could be observed. Repeated delivery with a 24h-interval would not achieve a lasting elevation of diffusion-based hypoxia in the tumour.

Inhibition of the oxygen enhancement effect (e.g. via hypoxic sensitizers) doubled the effectiveness of irradiation to lift hypoxia in the tumour. The oxygenation response of 2Gy x-rays with $O_{max} = 1$ closely matched the response to 4Gy under the effect of normal oxygen enhancement ($O_{max} = 2.9$). Repeated irradiation with suppressed oxygen effects led to a full reoxygenation of the tumour, both for repeated delivery of 2Gy or 4Gy. For larger doses of 4Gy the delivery of only 5 fractions was sufficient in order to delay the following rise of hypoxia, so that no radiobiologically hypoxic cells were present for the following fraction.

The dynamics of hypoxia in the model spheroid illustrated, that typically the diffusion-based reoxygenation will be lost before a follow-up dose is administered in 24h and 48h intervals. When the oxygen enhancement was suppressed, a fast and persistent oxygenation of the tumour was achieved. This suggests that hypoxic sensitizers can be strategically used in treatment planing and that shorter follow-up intervals should be considered for radiotherapy.
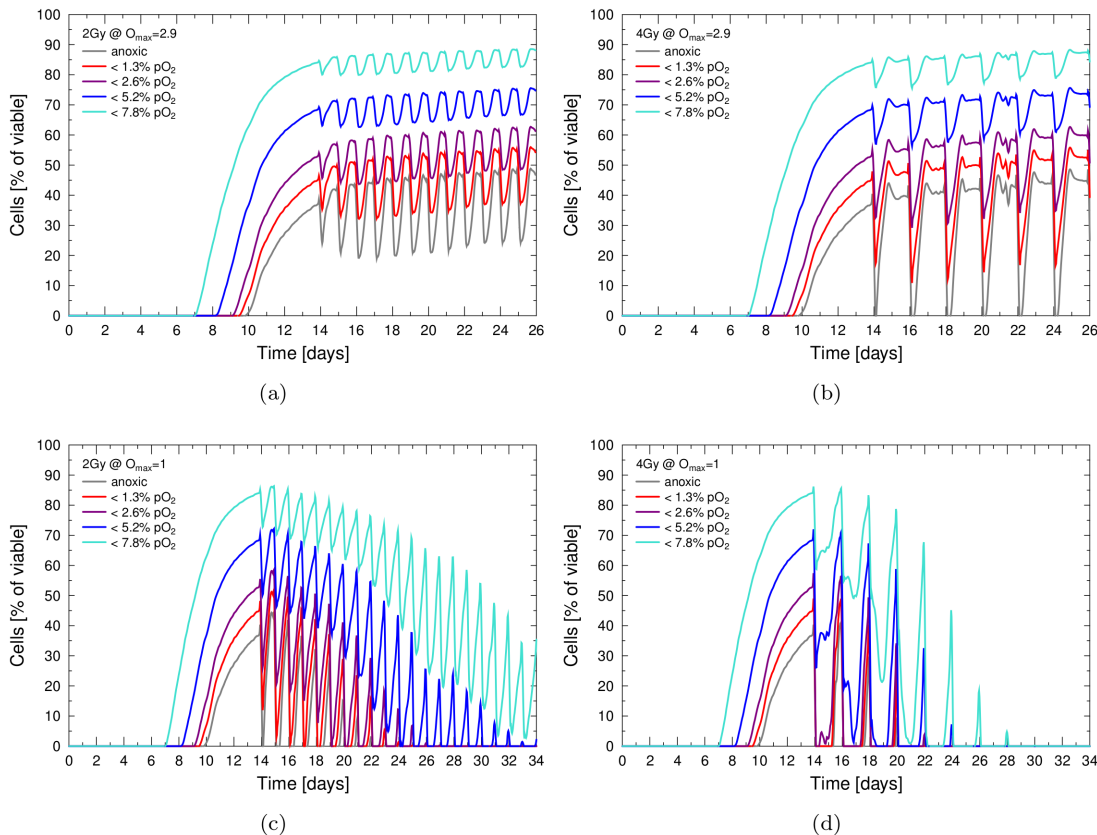
Fig 6. Reoxygenation during repeated radiation delivery. Persistence and stability of the reoxygenation response during multiple fractions and in prolonged irradiation regimes. Tumours where either irradiated with doses of 2 Gy per 24h (left column) or 4 Gy per 48h (right column). While a stable reoxygenation response can be observed, full reoxygenation is only possible if oxygen enhancement effects are suppressed via $O_{max} = 1$ as shown in the bottom row.

doi:10.1371/journal.pone.0133357.g006

Discussion

Using an agent-based tumour spheroid model, we demonstrated that the temporal and spatial variations of diffusion-based, chronic hypoxia are predictable on a qualitative as well as quantitative level. The obtained results can be directly compared to *in vitro* spheroid systems or xenograft tumour models for verification or falsification, using techniques such as EPRI to track the predicted reoxygenation response [24, 81]. The same techniques can be used to obtain data which is suitable for a fine-tuning of the model to specific cell lines. The current model can provide quantitative oxygen dynamics in spheroids and micro-regions of larger tumours, which was previously hard to achieve in most models [61]. It can thus be a first step towards a prospective productive combination with quantitative imaging techniques to be used in experimental treatment planing. The choice of cell line and the according variation of parameters only affected the results on a quantitative level, while the described qualitative phenomena were conserved for all reasonable variations of the parameters. Therefore the model yields a range of generic predictions which should be observable in a wide range of tumour systems.

In vivo, the hypoxia dynamics will be a mixture of multiple sources of hypoxia and can be extremely diverse [25], but the isolated influence of diffusion-based hypoxia could be studied both *in vitro* and *in silico* using spheroid experiments and simulations. While the current model disregards a range of mechanisms which are undoubtedly of great importance for the

treatment response of tumours, some of these mechanisms are suitable for integration within future *in silico* models. Explicit inclusion of the tumour microenvironment and the stromal background could allow for the study of resistance development. Single cell-based models can describe the selective pressure on cancer cells which is induced by hypoxic conditions and the according mutation of cells. The actions of immune agents can be directly included by a cell-based representation of immunocytes. The presented *in silico* model operates at reduced complexity but allows for a systematic, disentangled study of the influence of quiescent cells, oxygen enhancement, cell consumption and further effects on the reoxygenation dynamics. Thus a necessary simplifaction was performed as a first step on the way towards a more detailed model for experimental optimisation of treatment.

Implications of reoxygenation dynamics on treatment

With the help of our model system we demonstrated, that the complex response of tumours to radiotherapy leads to time-windows of transient reoxygenation. It is of vital importance that this effect is investigated in further studies to be eventually considered in treatment planing. The delivery of therapeutic measures as well as imaging schedules could be adapted to this diffusion-based oxygen dynamics. Delivery should be avoided during mainly hypoxic periods and instead enforced during reoxygenated times. The reoxygenation response of tumours can only be exploited if the timing is correct. For our sample tumour system the diffusion-based reoxygenation was on a timescale which would typically conflict with common fractionation intervals of 24 hours or 48 hours. In order to employ the reoxygenation effects, the simulation results suggest the investigation of shortened delivery intervals in order to avoid re-depletion of oxygen before the next therapeutic radiation fraction is applied. This finding should be studied in *in vitro* experiments as well as in more complex *in silico* models which are to be developed.

A very fast delivery of follow-up doses has been shown to be prohibitive due to the transient rise of hypoxic survivors directly in response to irradiation. If the next dose however is delivered too late, the benefits of reoxygenation are lost. This implies, that diffusion-based hypoxia defines a cell-type dependent interval for optimal use of the reoxygenation effects. A worthwhile investigation would be the delivery of a first radiation fraction as a trigger-dose which induces reoxygenation, which is followed by a correctly timed second "effector" dose which could thus fully exploit the induced effects of reoxygenation, before they are lost due to re-hypoxation.

Reoxygenation effects however are only one of the dynamic treatment-induced changes which will influence the overall treatment sensitivity of a tumour. They will be intermixed with other treatment-induced dynamic phenomena, such as cell reactivation, cell cycle synchronisation [53], changes in tissue diffusivity and so forth. The cell cycle dependent uptake of nutrients could further affect the reoxygenation, as cell cycle resynchronisation could induce macroscopic dynamics in consumption, which would lead to the according changes in the oxygenation. As a result, it appears mandatory to connect the oxygenation effects with a model for cell cycle effects as described in [52] or [42] in order to find optimal irradiation timings in respect to more than one phenomenon. The inclusion of immune effects and of stroma are further important steps in the development of an advanced model.

The suppression of the oxygen enhancement effect for irradiation had surprisingly strong effects on the oxygenation dynamics. If the maximum oxygen enhancement O_{max} was set to 1, that is either a hypoxic sensitizer is in effect or the cell line inherently shows a low dependency of radiation damage on oxygenation, the higher degree of cell killing would induce a pronounced reoxygenation. Thus the oxygen-dependence of radiation damage of the specific cells is of great importance for the reoxygenation timings of the tumour.

Any radio-sensitisation of hypoxic cells prior to treatment using hypoxic sensitizers could greatly enhance the reoxygenation which results from the radiation dose within the model. Even though clinical radiosensitizer trials have been mostly inconclusive, from no effect to a clear overall benefit, it seems that they can be used to increase the reoxygenation which can be induced by irradiation.

If radiation therapies are expected to fail to achieve a reoxygenation, this has to be known in advance. Other adequate measures to re-oxygenate radioresistant hypoxic regions, such as hypoxic sensitizers or hypoxia-specific therapies to eradicate hypoxic, radioresistant cell populations [8, 82], can be successfully employed in this case. This shows a high potential to combine hypoxic sensitizers and hypoxic cytotoxins with fractionated irradiation schedules to a more holistic treatment protocol.

A combination of hypoxic cytotoxins and irradiation seems to be fruitful, as hypoxia is not fully lifted by irradiation alone and the hypoxic cell population quickly rises again after treatment. At the same time, hypoxic cytotoxins can be administered as an adjuvant pre-treatment, in order to induce cell death in hypoxic regions, which in turn will re-oxygenate the tumour and increase the radiation efficiency.

As repeated cycles of oxygenation and hypoxia have been shown to increase the aggressiveness of tumours [4, 5], it may be beneficial to optimise treatment schedules in order to avoid predictable transient cycling reoxygenation and instead aim for a constant increase in oxygen concentration. This tactic could limit the development of aggressive strategies by the tumour in response to treatment [21]. Cell-based *in silico* models are well-suited to study this question, as mutation and the resulting increased aggressiveness can be included explicitly. Predictable oxygenation changes in response to radiotherapy also open up the possibility for a subsequent targeted therapy, which would be specifically based on altered gene expression [7].

The dynamics of hypoxia clearly show, that the results of PET-scanning will critically depend on the timing of imaging, especially when imaging is combined with therapy. Imaging-techniques must not only be used as initial prognostic marker, but must instead be used as active observable in order to update and optimise treatment delivery. Active radiation planing with OER dose-painting approaches must consequently not ignore the temporal variation of hypoxia on the finer scale of hours or even minutes [83]. A combination of imaging techniques and repeated, dynamic acquisition is necessary to tackle the "complexity of underlying tumour biology" [20, 84].

As neither patients nor tumours are static systems, adaptive radiotherapy and the live update of treatment plans has become a goal in clinical treatment. However, this requires an in-detail understanding of fundamental processes which happen within the tumour in response to external stimuli, such as radio- or chemotherapy. It has been stated regularly, that the spatio-temporal oxygen dynamics during radiotherapy need to be understood in order to predict an optimal timing of treatment and continued imaging [20, 30]. Spatio-temporal mathematical models, as proposed here, can be used to further this understanding and test the reaction of tumours under full control of all parameters. In combination with imaging such models can be used for the prediction of oxygen dynamics out of range of current temporal or spatial imaging resolution [36].

Supporting Information

S1 Fig. Complex oxygen dynamics in response to irradiation with 4Gy and $O_{max} = 1$. The local oxygen concentration in the spheroid varies in dependence on cell cycle status (quiescence), tissue density and cell death. Due to the dynamic interplay of these phenomena a

complex fluctuation of oxygenation levels is observed in response to treatment. Oxygen levels have been colour-coded as in Fig 3(c) and 3(d).
(TIFF)

Acknowledgments

Author Contributions

Conceived and designed the experiments: HK MB MM. Performed the experiments: HK. Analyzed the data: HK MM. Contributed reagents/materials/analysis tools: HK. Wrote the paper: HK MM.

References

1. Vaupel P. Tumor microenvironmental physiology and its implications for radiation oncology. Seminars in radiation oncology. 2004 Jul; 14(3):198–206. Available from: http://www.ncbi.nlm.nih.gov/pubmed/15254862 doi: 10.1016/j.semradonc.2004.04.008 PMID: 15254862

2. Höring E, Harter PN, Seznec J, Schittenhelm J, Bühring HJ, Bhattacharyya S, et al. The "go or grow" potential of gliomas is linked to the neuropeptide processing enzyme carboxypeptidase E and mediated by metabolic stress. Acta neuropathologica. 2012 Jul; 124(1):83–97. Available from: http://www.ncbi.nlm.nih.gov/pubmed/22249620 doi: 10.1007/s00401-011-0940-x PMID: 22249620

3. Bennewith KL, Dedhar S. Targeting hypoxic tumour cells to overcome metastasis. BMC cancer. 2011 Jan; 11(1):504. Available from: http://www.pubmedcentral.nih.gov/articlerender.fcgi?artid=3247198&tool = pmcentrez&rendertype = abstract doi: 10.1186/1471-2407-11-504 PMID: 22128892

4. Dewhirst MW, Cao Y, Moeller B. Cycling hypoxia and free radicals regulate angiogenesis and radiotherapy response. Nature reviews Cancer. 2008 Jun; 8(6):425–37. Available from: http://dx.doi.org/10.1038/nrc2397 http://www.ncbi.nlm.nih.gov/pubmed/18500244 doi: 10.1038/nrc2397 PMID: 18500244

5. Vaupel P. The role of hypoxia-induced factors in tumor progression. The oncologist. 2004 Jan; 9 Suppl 5(5):10–7. Available from: http://www.ncbi.nlm.nih.gov/pubmed/23026707 http://www.ncbi.nlm.nih.gov/pubmed/15591418 doi: 10.1634/theoncologist.9-90005-10 PMID: 15591418

6. Matsumoto S, Yasui H, Mitchell JB, Krishna MC. Imaging cycling tumor hypoxia. Cancer research. 2010 Dec; 70(24):10019–23. Available from: http://www.pubmedcentral.nih.gov/articlerender.fcgi?artid=3059188&tool = pmcentrez&rendertype = abstract doi: 10.1158/0008-5472.CAN-10-2821 PMID: 21159626

7. Cárdenas-Navia LI, Mace D, Richardson Ra, Wilson DF, Shan S, Dewhirst MW. The pervasive presence of fluctuating oxygenation in tumors. Cancer research. 2008 Jul; 68(14):5812–9. Available from: http://www.ncbi.nlm.nih.gov/pubmed/18632635 doi: 10.1158/0008-5472.CAN-07-6387 PMID: 18632635

8. Harada H. How can we overcome tumor hypoxia in radiation therapy? Journal of radiation research. 2011 Jan; 52(5):545–56. Available from: http://joi.jlc.jst.go.jp/JST.JSTAGE/jrr/11056?from=CrossRef http://www.ncbi.nlm.nih.gov/pubmed/21952313 doi: 10.1269/jrr.11056 PMID: 21952313

9. Leschner S, Weiss S. Salmonella-allies in the fight against cancer. Journal of molecular medicine (Berlin, Germany). 2010 Aug; 88(8):763–73. Available from: http://www.ncbi.nlm.nih.gov/pubmed/20526574 doi: 10.1007/s00109-010-0636-z

10. Carlin S, Humm JL. PET of hypoxia: current and future perspectives. Journal of nuclear medicine: official publication, Society of Nuclear Medicine. 2012 Aug; 53(8):1171–4. Available from: http://www.ncbi.nlm.nih.gov/pubmed/22789676 doi: 10.2967/jnumed.111.099770

11. Awwad HK, el Naggar M, Mocktar N, Barsoum M. Intercapillary distance measurement as an indicator of hypoxia in carcinoma of the cervix uteri. International journal of radiation oncology, biology, physics. 1986; 12:1329–1333. doi: 10.1016/0360-3016(86)90165-3 PMID: 3759554

12. Vaupel P, Kallinowski F, Okunieff P. Blood flow, oxygen and nutrient supply, and metabolic microenvironment of human tumors: a review. Cancer research. 1989 Dec; 49(23):6449–65. Available from: http://www.ncbi.nlm.nih.gov/pubmed/2684393 PMID: 2684393

13. Primeau AJ, Rendon A, Hedley D, Lilge L, Tannock IF. The distribution of the anticancer drug Doxorubicin in relation to blood vessels in solid tumors. Clinical cancer research: an official journal of the American Association for Cancer Research. 2005 Dec; 11(24 Pt 1):8782–8. Available from: http://www.ncbi.nlm.nih.gov/pubmed/16361566 doi: 10.1158/1078-0432.CCR-05-1664

14. Lyng H, Sundfør K, Rofstad EK. Oxygen tension in human tumours measured with polarographic needle electrodes and its relationship to vascular density, necrosis and hypoxia. Radiotherapy and oncology: journal of the European Society for Therapeutic Radiology and Oncology. 1997 Aug; 44(2):163–9. Available from: http://www.ncbi.nlm.nih.gov/pubmed/9288845 doi: 10.1016/S0167-8140(97)01920-8

15. Brown JM. Tumor microenvironment and the response to anticancer therapy. Cancer biology & therapy. 2002; 1(5):453–8. Available from: http://www.ncbi.nlm.nih.gov/pubmed/12496469 doi: 10.4161/cbt.1.5.157

16. Kaur B, Tan C, Brat DJ, Post DE, Van Meir EG. Genetic and hypoxic regulation of angiogenesis in gliomas. Journal of neuro-oncology. 2004 Nov; 70(2):229–43. Available from: http://www.springerlink.com/index/W45J340L849U3433.pdf http://www.ncbi.nlm.nih.gov/pubmed/15674480 doi: 10.1007/s11060-004-2752-5 PMID: 15674480

17. Kim IH, Brown JM. Reoxygenation and rehypoxiation in the SCCVII mouse tumor. International journal of radiation oncology, biology, physics. 1994 Jun; 29(3):493–7. Available from: http://www.ncbi.nlm.nih.gov/pubmed/8005805 doi: 10.1016/0360-3016(94)90444-8 PMID: 8005805

18. Busk M, Horsman MR, Overgaard J. Resolution in PET hypoxia imaging: voxel size matters. Acta oncologica (Stockholm, Sweden). 2008 Jan; 47(7):1201–10. Available from: http://www.ncbi.nlm.nih.gov/pubmed/18661432 doi: 10.1080/02841860802307716

19. Fenton BM, Lord EM, Paoni SF. Effects of radiation on tumor intravascular oxygenation, vascular configuration, development of hypoxia, and clonogenic survival. Radiation research. 2001 Feb; 155(2):360–8. Available from: http://www.ncbi.nlm.nih.gov/pubmed/11175672 doi: 10.1667/0033-7587(2001)155%5B0360:EOROTI%5D2.0.CO;2 PMID: 11175672

20. Thorwarth D, Alber M. Implementation of hypoxia imaging into treatment planning and delivery. Radiotherapy and oncology: journal of the European Society for Therapeutic Radiology and Oncology. 2010 Nov; 97(2):172–5. Available from: http://www.ncbi.nlm.nih.gov/pubmed/20570382 doi: 10.1016/j.radonc.2010.05.012

21. Bayer C, Shi K, Astner ST, Maftei CA, Vaupel P. Acute versus chronic hypoxia: why a simplified classification is simply not enough. International journal of radiation oncology, biology, physics. 2011 Jul; 80(4):965–8. Available from: http://www.ncbi.nlm.nih.gov/pubmed/21683887 doi: 10.1016/j.ijrobp.2011.02.049 PMID: 21683887

22. Brown JM, Giaccia AJ. The unique physiology of solid tumors: opportunities (and problems) for cancer therapy. Cancer research. 1998 Apr; 58(7):1408–16. Available from: http://www.ncbi.nlm.nih.gov/pubmed/9537241 PMID: 9537241

23. Badeer HS. Hemodynamics for medical students. Advances in physiology education. 2001; 25:44–52. PMID: 11824208

24. Yasui H, Matsumoto S, Devasahayam N, Munasinghe JP, Choudhuri R, Saito K, et al. Low-field magnetic resonance imaging to visualize chronic and cycling hypoxia in tumor-bearing mice. Cancer research. 2010 Aug; 70(16):6427–36. Available from: http://www.pubmedcentral.nih.gov/articlerender.fcgi?artid=2922437&tool = pmcentrez&rendertype = abstract doi: 10.1158/0008-5472.CAN-10-1350 PMID: 20647318

25. Hall EJ, Giaccia AJ. Radiobiology For The Radiologist. 6th ed. Lippincott Williams & Wilkins; 2005.

26. Harriss W, Bezak E, Yeoh E, Hermans M. Measurement of reoxygenation during fractionated radiotherapy in head and neck squamous cell carcinoma xenografts. Australasian physical & engineering sciences in medicine / supported by the Australasian College of Physical Scientists in Medicine and the Australasian Association of Physical Sciences in Medicine. 2010 Sep; 33(3):251–63. Available from: http://www.ncbi.nlm.nih.gov/pubmed/20878297 doi: 10.1007/s13246-010-0032-6

27. Alper T, Howard-Flanders P. Role of oxygen in modifying the radiosensitivity of E. coli B. Nature. 1956 Nov; 178(4540):978–9. Available from: http://www.ncbi.nlm.nih.gov/pubmed/13378491 doi: 10.1038/178978a0 PMID: 13378491

28. Yaes RJ, Patel P, Maruyama Y. On using the linear-quadratic model in daily clinical practice. International journal of radiation oncology, biology, physics. 1991; 20:1353–1362. PMID: 2045309

29. Staab A, Zukowski D, Walenta S, Scholz M, Mueller-Klieser W. Response of Chinese hamster v79 multicellular spheroids exposed to high-energy carbon ions. Radiation research. 2004 Feb; 161(2):219–27. doi: 10.1667/RR3113 PMID: 14731067

30. Lin A, Hahn SM. Hypoxia imaging markers and applications for radiation treatment planning. Seminars in nuclear medicine. 2012 Sep; 42(5):343–52. Available from: http://www.ncbi.nlm.nih.gov/pubmed/22840599 doi: 10.1053/j.semnuclmed.2012.04.002 PMID: 22840599

31. Minchinton AI, Tannock IF. Drug penetration in solid tumours. Nature reviews Cancer. 2006 Aug; 6(8):583–92. Available from: http://www.ncbi.nlm.nih.gov/pubmed/16862189 doi: 10.1038/nrc1893 PMID: 16862189

32. Krause BJ, Beck R, Souvatzoglou M, Piert M. PET and PET/CT studies of tumor tissue oxygenation. The quarterly journal of nuclear medicine and molecular imaging: official publication of the Italian Association of Nuclear Medicine (AIMN) [and] the International Association of Radiopharmacology (IAR), [and] Section of the Society of Radiopharmaceutica 2006 Mar; 50(1):28–43. Available from: http://www.ncbi.nlm.nih.gov/pubmed/16557202

33. Horsman MR, Mortensen LS, Petersen JrB, Busk M, Overgaard J. Imaging hypoxia to improve radiotherapy outcome. Nature reviews Clinical oncology. 2012 Dec; 9(12):674–87. Available from: http://www.nature.com/nrclinonc/journal/v9/n12/pdf/nrclinonc.2012.171.pdf doi: 10.1038/nrclinonc.2012.171 PMID: 23149893

34. Bache M, Kappler M, Said HM, Staab A, Vordermark D. Detection and specific targeting of hypoxic regions within solid tumors: current preclinical and clinical strategies. Current medicinal chemistry. 2008 Jan; 15(4):322–38. Available from: http://www.ncbi.nlm.nih.gov/pubmed/18288988 doi: 10.2174/092986708783497391 PMID: 18288988

35. Battaglini CL, Mills RC, Phillips BL, Lee JT, Story CE, Nascimento MGB, et al. Positron emission tomography to assess hypoxia and perfusion in lung cancer. 2014; 5(5):824–845.

36. Zheng X, Wang X, Mao H, Wu W, Liu B, Jiang X. Hypoxia-specific ultrasensitive detection of tumours and cancer cells in vivo. Nature communications. 2015; 6:5834. doi: 10.1038/ncomms6834 PMID: 25556360

37. Kelada OJ, Carlson DJ. Molecular imaging of tumor hypoxia with positron emission tomography. Radiation research. 2014; 181:335–49. Available from: http://www.ncbi.nlm.nih.gov/pubmed/24673257 doi: 10.1667/RR13590.1 PMID: 24673257

38. Pampaloni F, Ansari N, Stelzer EHK. High-resolution deep imaging of live cellular spheroids with light-sheet-based fluorescence microscopy. Cell and tissue research. 2013 Feb;p. 161–177. Available from: http://www.ncbi.nlm.nih.gov/pubmed/23443300 doi: 10.1007/s00441-013-1589-7 PMID: 23443300

39. Ansari N, Müller S, Stelzer EHK, Pampaloni F. Quantitative 3D cell-based assay performed with cellular spheroids and fluorescence microscopy. Methods in cell biology. 2013 Jan; 113:295–309. Available from: http://www.ncbi.nlm.nih.gov/pubmed/23317907 doi: 10.1016/B978-0-12-407239-8.00013-6 PMID: 23317907

40. Titz B, Jeraj R. An imaging-based tumour growth and treatment response model: investigating the effect of tumour oxygenation on radiation therapy response. Physics in medicine and biology. 2008 Sep; 53(17):4471–88. Available from: http://www.pubmedcentral.nih.gov/articlerender.fcgi?artid=2819145&tool = pmcentrez&rendertype = abstract doi: 10.1088/0031-9155/53/17/001 PMID: 18677042

41. Hatzikirou H, Alfonso JCL, Stern C, Weiss S. Cancer therapeutic potential of combinatorial immuno- and vaso-modulatory interventions. arxivorg. 2015;p. 1–31.

42. Powathil GG, Gordon KE, Hill La, Chaplain MaJ. Modelling the effects of cell-cycle heterogeneity on the response of a solid tumour to chemotherapy: biological insights from a hybrid multiscale cellular automaton model. Journal of theoretical biology. 2012 Sep; 308:1–19. Available from: http://www.ncbi.nlm.nih.gov/pubmed/22659352 doi: 10.1016/j.jtbi.2012.05.015 PMID: 22659352

43. Powathil GG, Adamson DJa, Chaplain MaJ. Towards predicting the response of a solid tumour to chemotherapy and radiotherapy treatments: clinical insights from a computational model. PLoS computational biology. 2013 Jul; 9(7):e1003120. Available from: http://www.pubmedcentral.nih.gov/articlerender.fcgi?artid=3708873&tool = pmcentrez&rendertype = abstract doi: 10.1371/journal.pcbi.1003120 PMID: 23874170

44. Carlson DJ, Keall PJ, Loo BW, Chen ZJ, Brown JM. Hypofractionation results in reduced tumor cell kill compared to conventional fractionation for tumors with regions of hypoxia. International journal of radiation oncology, biology, physics. 2011 Mar; 79(4):1188–95. Available from: http://www.pubmedcentral.nih.gov/articlerender.fcgi?artid=3053128&tool = pmcentrez&rendertype = abstract doi: 10.1016/j.ijrobp.2010.10.007 PMID: 21183291

45. Daşu A, Toma-Daşu I, Karlsson M. Theoretical simulation of tumour oxygenation and results from acute and chronic hypoxia. Physics in medicine and biology. 2003 Sep; 48(17):2829–42. Available from: http://www.ncbi.nlm.nih.gov/pubmed/14516104 doi: 10.1088/0031-9155/48/17/307

46. Toma-Daşu I, Daşu A, Karlsson M. The relationship between temporal variation of hypoxia, polaro-graphic measurements and predictions of tumour response to radiation. Physics in medicine and biol-ogy. 2004 Oct; 49(19):4463–75. Available from: http://stacks.iop.org/0031-9155/49/i=19/a=002?key = crossref.197fef6822e0e75a8b97fce1ca3fe210 http://www.ncbi.nlm.nih.gov/pubmed/15552411 doi: 10.1088/0031-9155/49/19/002

47. Powathil G, Kohandel M, Milosevic M, Sivaloganathan S. Modeling the spatial distribution of chronic tumor hypoxia: implications for experimental and clinical studies. Computational and mathematical methods in medicine. 2012 Jan; 2012:410602. Available from: http://www.pubmedcentral.nih.gov/articlerender.fcgi?artid=3287099&tool = pmcentrez&rendertype = abstract doi: 10.1155/2012/410602 PMID: 22400049

48. Alarcón T, Byrne HM, Maini PK. Towards whole-organ modelling of tumour growth. Progress in bio-physics and molecular biology. 2004; 85(2–3):451–72. Available from: http://www.ncbi.nlm.nih.gov/pubmed/15142757 PMID: 15142757

49. Dionysiou DD, Stamatakos GS, Uzunoglu NK, Nikita KS, Marioli A. A four-dimensional simulation model of tumour response to radiotherapy in vivo: parametric validation considering radiosensitivity, genetic profile and fractionation. J Theor Biol. 2004 Sep; 230(1):1–20. Available from: http://dx.doi.org/10.1016/j.jtbi.2004.03.024 http://www.ncbi.nlm.nih.gov/pubmed/15275995 doi: 10.1016/j.jtbi.2004.03.024 PMID: 15275995

50. Angus SD, Piotrowska MJ. A matter of timing: identifying significant multi-dose radiotherapy improve-ments by numerical simulation and genetic algorithm search. PloS one. 2014; 9(12):e114098. doi: 10.1371/journal.pone.0114098 PMID: 25460164

51. López Alfonso JC, Jagiella N, Núñez L, Herrero Ma, Drasdo D. Estimating dose painting effects in radiotherapy: A mathematical model. PLoS ONE. 2014; 9(2).

52. Kempf H, Bleicher M, Meyer-Hermann M. Spatio-temporal cell dynamics in tumour spheroid irradiation. The European Physical Journal D. 2010 Jun; 60(1):177–193. Available from: http://www.springerlink.com/index/10.1140/epjd/e2010-00178-4 doi: 10.1140/epjd/e2010-00178-4

53. Kempf H, Hatzikirou H, Bleicher M, Meyer-Hermann M. In silico analysis of cell cycle synchronisation effects in radiotherapy of tumour spheroids. PLoS computational biology. 2013 Nov; 9(11):e1003295. Available from: http://www.pubmedcentral.nih.gov/articlerender.fcgi?artid=3828142&tool = pmcentrez&rendertype = abstract doi: 10.1371/journal.pcbi.1003295 PMID: 24244120

54. Schaller G, Meyer-Hermann M. Kinetic and dynamic Delaunay tetrahedralizations in three dimensions. Computer Physics Communications. 2004; 162:9–23. doi: 10.1016/j.cpc.2004.06.066

55. Beyer T, Schaller G, Deutsch A, Meyer-Hermann M. Parallel dynamic and kinetic regular triangulation in three dimensions. Computer Physics Communications. 2005 Nov; 172(2):86–108. Available from: http://linkinghub.elsevier.com/retrieve/pii/S0010465505003991 doi: 10.1016/j.cpc.2005.06.009

56. Schaller G, Meyer-Hermann M. Multicellular tumor spheroid in an off-lattice Voronoi-Delaunay cell model. Physical review E, Statistical, nonlinear, and soft matter physics. 2005 May; 71(5 Pt 1):051910. Available from: http://link.aps.org/doi/10.1103/PhysRevE.71.051910 http://www.ncbi.nlm.nih.gov/pubmed/16089574 doi: 10.1103/PhysRevE.71.051910 PMID: 16089574

57. Chu YS, Dufour S, Thiery JP, Perez E, Pincet F. Johnson-Kendall-Roberts theory applied to living cells. Physical review letters. 2005 Jan; 94(2):28102. Available from: http://www.ncbi.nlm.nih.gov/pubmed/15698233 doi: 10.1103/PhysRevLett.94.028102

58. Beyer T, Meyer-Hermann M. Modeling emergent tissue organization involving high-speed migrating cells in a flow equilibrium. Physical review E, Statistical, nonlinear, and soft matter physics. 2007 Aug; 76(2 Pt 1):021929. Available from: http://www.ncbi.nlm.nih.gov/pubmed/17930087 doi: 10.1103/PhysRevE.76.021929 PMID: 17930087

59. Scifoni E, Tinganelli W, Weyrather WK, Durante M, Maier a, Krämer M. Including oxygen enhancement ratio in ion beam treatment planning: model implementation and experimental verification. Physics in medicine and biology. 2013 Jun; 58(11):3871–95. Available from: http://www.ncbi.nlm.nih.gov/pubmed/23681217 doi: 10.1088/0031-9155/58/11/3871 PMID: 23681217

60. Wehrle JP, Ng CE, McGovern KA, Aiken NR, Shungu DC, Chance EM, et al. Metabolism of alternative substrates and the bioenergetic status of EMT6 tumor cell spheroids. NMR in biomedicine. 2000 Oct; 13(6):349–60. Available from: http://www.ncbi.nlm.nih.gov/pubmed/11002314 doi: 10.1002/1099-1492(200010)13:6%3C349::AID-NBM652%3E3.3.CO;2-O PMID: 11002314

61. Toma-Dasu I, Dasu A. Modelling tumour oxygenation, reoxygenation and implications on treatment out-come. Computational and mathematical methods in medicine. 2013 Jan; 2013:141087. Available from:

http://www.pubmedcentral.nih.gov/articlerender.fcgi?artid=3557613&tool = pmcentrez&rendertype = abstract doi: 10.1155/2013/141087 PMID: 23401721

62. Kallinowski F, Tyler G, Mueller-Klieser W, Vaupel P. Growth-related changes of oxygen consumption rates of tumor cells grown in vitro and in vivo. Journal of cellular physiology. 1989 Jan; 138(1):183–91. Available from: http://www.ncbi.nlm.nih.gov/pubmed/2910882 doi: 10.1002/jcp.1041380124 PMID: 2910882

63. Freyer JP, Sutherland RM. A reduction in the in situ rates of oxygen and glucose consumption of cells in EMT6/Ro spheroids during growth. J Cell Physiol. 1985 Sep; 124(3):516–524. Available from: http://dx.doi.org/10.1002/jcp.1041240323 http://www.ncbi.nlm.nih.gov/pubmed/4044662 doi: 10.1002/jcp.1041240323 PMID: 4044662

64. Cotran RS, Kumar V, Collins T, Robbins SL, Cotran R S KV. Robbins Pathologic Basis of Disease. 5th ed. Robbins Pathology Series. Saunders, Philadelphia; 1999.

65. Stein WD. Channels, carriers, and pumps: An introduction to membrane transport. Academic Press (San Diego); 1990.

66. Casciari JJ, Sotirchos SV, Sutherland RM. Glucose Diffusivity in Multicellular Tumor Spheroids. Cancer Research. 1988 Jul; 48(14):3905–3909. Available from: http://www.ncbi.nlm.nih.gov/pubmed/3383189 PMID: 3383189

67. Grote J, Süsskind R, Vaupel P. Oxygen diffusivity in tumor tissue (DS-carcinosarcoma) under temperature conditions within the range of 20–40 degrees C. Pflügers Archiv: European journal of physiology. 1977 Nov; 372(1):37–42. Available from: http://www.ncbi.nlm.nih.gov/pubmed/563582 PMID: 563582

68. Festjens N, Vanden Berghe T, Vandenabeele P. Necrosis, a well-orchestrated form of cell demise: signalling cascades, important mediators and concomitant immune response. Biochimica et biophysica acta. 2006; 1757(9–10):1371–87. Available from: http://www.ncbi.nlm.nih.gov/pubmed/16950166 doi: 10.1016/j.bbabio.2006.06.014 PMID: 16950166

69. Saraste A, Pulkki K. Morphologic and biochemical hallmarks of apoptosis. Cardiovascular research. 2000 Feb; 45(3):528–37. Available from: http://www.ncbi.nlm.nih.gov/pubmed/10728374 doi: 10.1016/S0008-6363(99)00384-3 PMID: 10728374

70. Zacharaki EI, Stamatakos GS, Nikita KS, Uzunoglu NK. Simulating growth dynamics and radiation response of avascular tumour spheroids-model validation in the case of an EMT6/Ro multicellular spheroid. Computer methods and programs in biomedicine. 2004 Dec; 76(3):193–206. Available from: http://www.ncbi.nlm.nih.gov/pubmed/15501506 doi: 10.1016/j.cmpb.2004.07.003 PMID: 15501506

71. Helmlinger G, Netti PA, Lichtenbeld HC, Melder RJ, Jain RK. Solid stress inhibits the growth of multicellular tumor spheroids. Nature biotechnology. 1997 Aug; 15(8):778–83. Available from: http://www.ncbi.nlm.nih.gov/pubmed/9255794 doi: 10.1038/nbt0897-778 PMID: 9255794

72. Sinclair WK. Cyclic x-ray responses in mammalian cells in vitro. Radiation research. 1968 Mar; 33(3): 620–43. Available from: http://www.ncbi.nlm.nih.gov/pubmed/4867897 doi: 10.2307/3572419 PMID: 4867897

73. Masunaga S, Ono K, Abe M. A method for the selective measurement of the radiosensitivity of quiescent cells in solid tumors–combination of immunofluorescence staining to BrdU and micronucleus assay. Radiation research. 1991 Mar; 125(3):243–7. Available from: http://www.ncbi.nlm.nih.gov/pubmed/1705716 doi: 10.2307/3578105 PMID: 1705716

74. Masunaga SI, Ando K, Uzawa A, Hirayama R, Furusawa Y, Koike S, et al. Responses of total and quiescent cell populations in solid tumors to carbon ion beam irradiation (290 MeV/u) in vivo. Radiation medicine. 2008 Jun; 26(5):270–7. Available from: http://www.ncbi.nlm.nih.gov/pubmed/18661211 doi: 10.1007/s11604-008-0227-x PMID: 18661211

75. Buffa FM, West C, Byrne K, Moore JV, Nahum aE. Radiation response and cure rate of human colon adenocarcinoma spheroids of different size: the significance of hypoxia on tumor control modelling. International journal of radiation oncology, biology, physics. 2001 Mar; 49(4):1109–18. Available from: http://www.ncbi.nlm.nih.gov/pubmed/11240253 doi: 10.1016/S0360-3016(00)01533-9 PMID: 11240253

76. Hill aV. The Diffusion of Oxygen and Lactic Acid through Tissues. Proceedings of the Royal Society B: Biological Sciences. 1928 Dec; 104(728):39–96. Available from: http://rspb.royalsocietypublishing.org/cgi/doi/10.1098/rspb.1928.0064 doi: 10.1098/rspb.1928.0064

77. Wenzl T, Wilkens JJ. Modelling of the oxygen enhancement ratio for ion beam radiation therapy. Physics in medicine and biology. 2011 Jun; 56(11):3251–68. Available from: http://www.ncbi.nlm.nih.gov/pubmed/21540489 doi: 10.1088/0031-9155/56/11/006 PMID: 21540489

78. Helmlinger G, Yuan F, Dellian M, Jain RK. Interstitial pH and pO2 gradients in solid tumors in vivo: high-resolution measurements reveal a lack of correlation. Nature medicine. 1997 Feb; 3(2):177–82. Available from: http://www.ncbi.nlm.nih.gov/pubmed/9018236 doi: 10.1038/nm0297-177 PMID: 9018236

79. Jain RK, Stylianopoulos T. Delivering nanomedicine to solid tumors. Nature reviews Clinical oncology. 2010 Nov; 7(11):653–64. Available from: http://www.pubmedcentral.nih.gov/articlerender.fcgi?artid= 3065247&tool = pmcentrez&rendertype = abstract doi: 10.1038/nrclinonc.2010.139 PMID: 20838415

80. Ryan RM, Green J, Williams PJ, Tazzyman S, Hunt S, Harmey JH, et al. Bacterial delivery of a novel cytolysin to hypoxic areas of solid tumors. Gene therapy. 2009 Mar; 16(3):329–39. Available from: http://www.ncbi.nlm.nih.gov/pubmed/19177133 doi: 10.1038/gt.2008.188 PMID: 19177133

81. Tung YC, Hsiao AY, Allen SG, Torisawa Ys, Ho M, Takayama S. High-throughput 3D spheroid culture and drug testing using a 384 hanging drop array. The Analyst. 2011 Feb; 136(3):473–8. Available from: http://pubs.rsc.org/en/content/articlehtml/2011/an/c0an00609b doi: 10.1039/C0AN00609B PMID: 20967331

82. Yahiro T, Masui S, Kubota N, Yamada K, Kobayashi A, Kishii K. Effects of hypoxic cell radiosensitizer doranidazole (PR-350) on the radioresponse of murine and human tumor cells in vitro and in vivo. Journal of radiation research. 2005 Sep; 46(3):363–72. Available from: http://www.ncbi.nlm.nih.gov/ pubmed/16210793 doi: 10.1269/jrr.46.363 PMID: 16210793

83. Grégoire V, Haustermans K, Geets X, Roels S, Lonneux M. PET-based treatment planning in radiotherapy: a new standard? Journal of nuclear medicine: official publication, Society of Nuclear Medicine. 2007 Jan; 48 Suppl 1(1):68S–77S. Available from: http://www.ncbi.nlm.nih.gov/pubmed/17204722

84. Bentzen SrM. Theragnostic imaging for radiation oncology: dose-painting by numbers. The lancet oncology. 2005 Feb; 6(2):112–7. Available from: http://www.thelancet.com/journals/a/article/PIIS1470- 2045(05)01737-7/fulltext doi: 10.1016/S1470-2045(05)01737-7 PMID: 15683820